Functional diffusion map: A noninvasive MRI biomarker for early stratification of clinical brain tumor response

Bradford A. Moffat*, Thomas L. Chenevert*†, Theodore S. Lawrence‡, Charles R. Meyer*, Timothy D. Johnson§, Qian Dong*, Christina Tsien‡, Suresh Mukherji*, Douglas J. Quint*, Stephen S. Gebarski*, Patricia L. Robertson¶, Larry R. Junck‖, Alnawaz Rehemtulla†‡, and Brian D. Ross*†**

Departments of *Radiology, ‡Radiation Oncology, ‖Neurology, ¶Pediatrics, and §Biostatistics, University of Michigan School of Medicine, Ann Arbor, MI 48109

Communicated by George J. Todaro, Targeted Growth, Inc., Seattle, WA, February 25, 2005 (received for review November 24, 2004)

Assessment of radiation and chemotherapy efficacy for brain cancer patients is traditionally accomplished by measuring changes in tumor size several months after therapy has been administered. The ability to use noninvasive imaging during the early stages of fractionated therapy to determine whether a particular treatment will be effective would provide an opportunity to optimize individual patient management and avoid unnecessary systemic toxicity, expense, and treatment delays. We investigated whether changes in the Brownian motion of water within tumor tissue as quantified by using diffusion MRI could be used as a biomarker for early prediction of treatment response in brain cancer patients. Twenty brain tumor patients were examined by standard and diffusion MRI before initiation of treatment. Additional images were acquired 3 weeks after initiation of chemo- and/or radiotherapy. Images were coregistered to pretreatment scans, and changes in tumor water diffusion values were calculated and displayed as a functional diffusion map (fDM) for correlation with clinical response. Of the 20 patients imaged during the course of therapy, 6 were classified as having a partial response, 6 as stable disease, and 8 as progressive disease. The fDMs were found to predict patient response at 3 weeks from the start of treatment, revealing that early changes in tumor diffusion values could be used as a prognostic indicator of subsequent volumetric tumor response. Overall, fDM analysis provided an early biomarker for predicting treatment response in brain tumor patients.

diffusion MRI | therapeutic response

It is projected that in 2004, ≈18,400 new cases of primary brain cancer will be diagnosed in the United States and 12,690 people will die of the disease (1). Malignant gliomas are the most common of these brain tumors and have a high mortality rate and short median length of survival (40.9 weeks) (2). In terms of biology, treatment, and prognosis, brain tumors are a heterogeneous group of neoplasms (3). The early identification of tumors responsive to therapy versus those that are not would greatly facilitate modifying an ineffective treatment regimen in a more timely fashion than is usual with standard measurements of tumor response.

Current assessment of CNS tumor treatment response relies on evaluating changes in the maximal cross-sectional area of the tumor or the product of the maximal perpendicular tumor diameters (4, 5) weeks to months after the conclusion of a therapeutic protocol (6, 7). Several noninvasive imaging methods [positron-emission tomography, single-photon emission computerized tomography, magnetic resonance (MR) spectroscopy and diffusion MRI] are being evaluated for assessing early therapeutic response that are independent of late changes in tumor volume (8–13). Diffusion MRI detection of cancer treatment response was first successfully reported in a rodent brain tumor model treated with chemotherapy (13). The hypothesis underlying this approach is that changes in tumor water diffusion occur after successful treatment that can be attributed to changes in cell density (13–19), resulting from necrosis and/or apoptotic processes (Fig. 1*A*). Moreover, initial regions of high extracellular water content (e.g., intratumoral edema, necrosis, and/or cysts) may decrease in volume because of dynamic reorganization of the heterogeneous tumor structure after treatment (Fig. 1*B*). The change in cell density due to cell kill along with tissue reorganization may lead to heterogeneous changes in the underlying tissue morphology (e.g., ratio of intra- to extracellular water), resulting in spatially varying changes in tumor apparent diffusion coefficient (ADC) values.

Changes detected in mean tumor ADC values after treatment in rodent tumor models revealed that this approach has merit for preclinical drug development studies as a sensitive and early predictor of therapeutic efficacy (13, 20–27). However, clinical utility of this approach has been hampered because of tumor heterogeneity and suboptimal methods of digital image analysis (28–32). Furthermore, although these preliminary studies have shown correlations between ADC change and tumor response, a definitive study demonstrating the ability of diffusion MRI to predict response has not been reported. Prediction of tumor response is critical for diffusion MRI to become a validated clinical biomarker of early treatment response.

We investigated whether diffusion MRI could be used to provide early detection of the therapeutic response of malignant brain tumors in humans as was observed in rodent brain tumors (13, 28). In this study, we prospectively compared tumor diffusion values at 3 weeks after initiation of therapy with pretreatment images to quantitate therapy-induced changes in ADC. A diagramatic representation of this approach is shown in Fig. 1*C*, where the two image datasets are coregistered and computationaly analyzed (see *Methods*) to yield functional diffusion maps (fDMs), which consist of a color overlay image of therapeutic-induced ADC change within the tumor. The fDM provides the ability to objectively segment the tumor into three color regions based on the magnitude and direction of ADC change. The volumes of these regions are also displayed as a scatter plot and were found to correlate with subsequent tumor response (post-treatment change in tumor size by using standard radiographic criteria). Statistical analysis of this data revealed that this fDM

Freely available online through the PNAS open access option.

Abbreviations: ADC, apparent diffusion coefficient; fDM, functional diffusion map; MR, magnetic resonance; PD, progressive disease; PR, partial response; SD, stable disease; V_B, blue voxels; V_G, green voxels; V_R, red voxels.

†T.L.C., A.R., and B.D.R. have a financial interest in the underlying technology (patent no. 6,567,684). Furthermore, this technology is licensed to a company in which A.R. and B.D.R. have a financial interest.

**To whom correspondence should be addressed. E-mail: bdross@umich.edu.

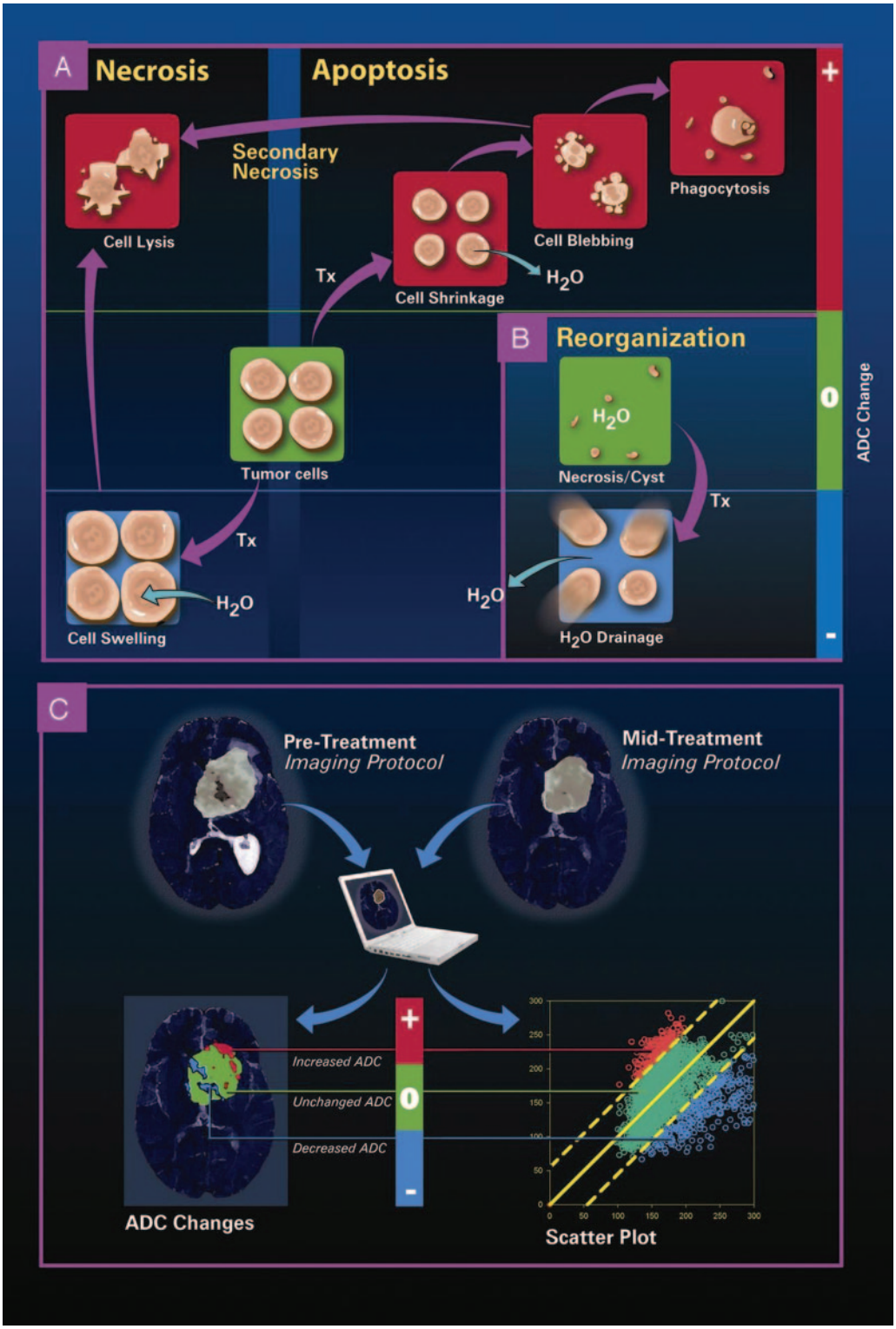

Fig. 1. Biological processes proposed to be involved in therapeutic-induced changes in tumor ADC values along with a pictorial description of the fDM analytical process. (*A*) A schematic representation of the dynamic biological processes associated with changes (increase or decrease) in tumor water diffusion values. Tumor cells within an image voxel have several fates during treatment. Cells can be resistant to therapy (unaltered ADC, green) or can undergo necrosis initiated by a transient cell swelling (decreased ADC, blue). Cell enlargement (swelling) can also be associated with mitotic catastrophe or a reduction in tumor blood flow resulting in focal ischemia/hypoxia (decreased ADC, blue). These processes can eventually progress to cell lysis and necrosis (increased ADC, red). Cells can also undergo apoptosis involving cell shrinkage and blebbing followed by phagocytosis (increased ADC, red). (*B*) The concept that necrotic or cystic regions of a tumor can undergo drainage (displacement) of water as cells move into the region resulting in a drop in diffusion values (decreased ADC, blue) is summarized. (*C*) Diffusion MRI data undergo digital image postprocessing and analysis that involves coregistration of images before and during treatment. Data are used to generate a three-color overlay representing regions in which tumor ADC values are unchanged (green voxels), significantly increased (red voxels), or significantly decreased (blue voxels). This data can also be presented in a scatter plot and percentages assigned to the three defined ADC regions, allowing quantitative assessment of overall changes in tumor ADC values.

approach could be used as a biomarker to predict early tumor response to therapy.

Methods

Patients. Patients with unresectable primary brain tumors were recruited to participate in a longitudinal clinical imaging trial to test the efficacy of the fDM approach for assessment of treatment response. To be eligible for the trial, patients were required to have a malignant brain tumor confirmed by histology as glioblastoma multiforme, astrocytoma, anaplastic astrocytoma, anaplastic oligodendroglioma, germ cell, or primitive neuroectodermal tumor, either at the initial diagnosis or at the time of tumor relapse. In addition, patients were only included if they were to receive radiation, chemotherapy, or a combination of both. Twenty patients were recruited into the study and underwent pretreatment diffusion MRI as well as the standard MRI (fluid attenuated inversion recovery, T2-weighted MRI, and gadolinium-enhanced T1-weighted MRI). All patients also underwent the same studies 3 weeks after initiation of therapy and follow-up standard MRI was accomplished to determine radiological response after completion of therapy.

Radiographic treatment outcomes based on the "crossed diameter product" were classified according to the World Health Organization criteria as follows: CR, complete resolution of tumor contrast enhancement and cessation of all steroids; partial response (PR), >50% decrease in tumor volume observed at least 4 weeks after the conclusion of therapy and on stable or decreased dosage of steroids; stable disease (SD), <50% decrease or a <25% increase in tumor volume and stable or decreased dose of steroids; and progressive disease (PD), >25% increase in tumor volume and on stable or increased dose of steroids. Written informed consent was obtained from all subjects, and all images and medical records were obtained according to protocols approved by the University of Michigan Medical School Institutional Review Board.

MRI. Water diffusion-sensitive images of the brain were acquired on a 1.5 T human MRI system (General Electric Medical Systems, Milwaukee, WI); capable of single-shot echo-planar imaging (EPI) (33). The diffusion spin-echo EPI sequence (TR/TE = 10,000/100 msec) was set to acquire at least 14, 6-mm-thick, contiguous axial-oblique sections through the brain at a given diffusion sensitivities (i.e., "b factors") along all three orthogonal directions. A set of diffusion-weighted images at high diffusion sensitivity (b2 = 1,000 sec/mm^2) and low sensitivity b1 $\cong$ 0 (i.e., T2-weighted) were collected in 80 sec. Mean ADC maps were then calculated from the three orthogonal directions because this quantity represents a rotationally invariant scalar of the diffusion tensor (34). That is, ADC maps were then calculated according to

$$ADC_i = \frac{1}{(b2 - b1)} \log_e \left[\frac{S_{b1}}{S_{b2}} \right], \qquad [1]$$

where S_{b1} and S_{b2} are signal intensities at low- and high-diffusion weighting, respectively, and i is the direction along which the diffusion sensitization gradients were placed (x, y, and z). These ADC maps were then averaged to calculate the scalar invariant mean ADC:

$$ADC_o = \frac{[ADC_x + ADC_y + ADC_z]}{3}. \qquad [2]$$

The quantity, ADC_o, is a scalar invariant of the diffusion tensor, thus, it avoids complexities introduced by anisotropy in brain tissue (34–36).

Image Analysis. All MR images were spatially coregistered by using the pretreatment T2 weighted images as the reference dataset. This step allowed all images of a given patient to be viewed and analyzed from a fixed frame of reference. The coregistration was performed by using a "mutual information for automatic multimodality image fusion" (MIAMI FUSE) algorithm (37). After this coregistration, brain tumors were manually segmented on the images by neuroradiologists. For this study, tumor tissue was defined as tissue that was either contrast-enhanced on T1-weighted images or was contained within a "ring" enhancement. Tumor cross-sectional diameters were measured by the radiologists for calculation of the crossed diameter product.

For each patient, diffusion changes were quantified by using a multiparametric analysis. ADC values of each voxel within the tumor fDM at 3 weeks were plotted as a function of their pretherapy ADC (Fig. 1*C*, scatter plot). Because shrinkage or growth of the tumor during the time between scans may have occurred, only voxels that were present in both the pretherapy and posttherapy tumor volumes as segmented by radiologists were included. All tumor voxels were objectively segmented into three different categories: red voxels (V_R) for which the ADC increased significantly, blue voxels (V_B) for which the ADC decreased significantly, and green voxels (V_G) for which the ADC did not change significantly. The three-color fDM was overlayed on the anatomical image. The mean of 15 independent observation prediction intervals (see statistical analysis below) was used as the significance threshold. The total volume of the voxels within each of the three categories (red, blue, and green) was calculated for each patient at week 3 (Fig. 1*C*) and normalized against the total tumor volume to give three normalized tumor volume segments for each patient V_R, V_B, and V_G, respectively.

Statistical Analysis. The thresholds for determining whether there was a significant change in diffusion within a voxel were determined empirically from 15 coregistered data sets from five different patients. For each coregistered data set, a volume of interest >50 ml within the contralateral brain containing a range

Table 1. Patient summary

Response	Tumor type	Age	Gender	Therapy
PR	AA	41	M	Radiation
	AO	37	M	Chemotherapy
	AO	56	F	Radiation
	Germ cell	10	F	Chemotherapy
	Germ cell	15	M	Chemotherapy
	PNET	8	F	Chemotherapy
SD	AA	36	M	Radiation
	AO	47	F	Radiation
	GBM	40	F	Radiation
	GBM	67	F	Radiation
	GBM	28	M	Radiation
	PNET	13	F	Combination
PD	A	44	F	Radiation
	A	45	F	Combination
	A	63	F	Radiation
	AO	64	M	Radiation
	GBM	46	M	Radiation
	GBM	20	M	Radiation
	GBM	42	F	Radiation
	GBM	45	F	Chemotherapy

AA, anaplastic astrocytoma; AO, anaplastic oligodendroglioma; PNET, primitive neuroectodermal tumor; GBM, glioblastoma multiforme; A, astrocytoma.

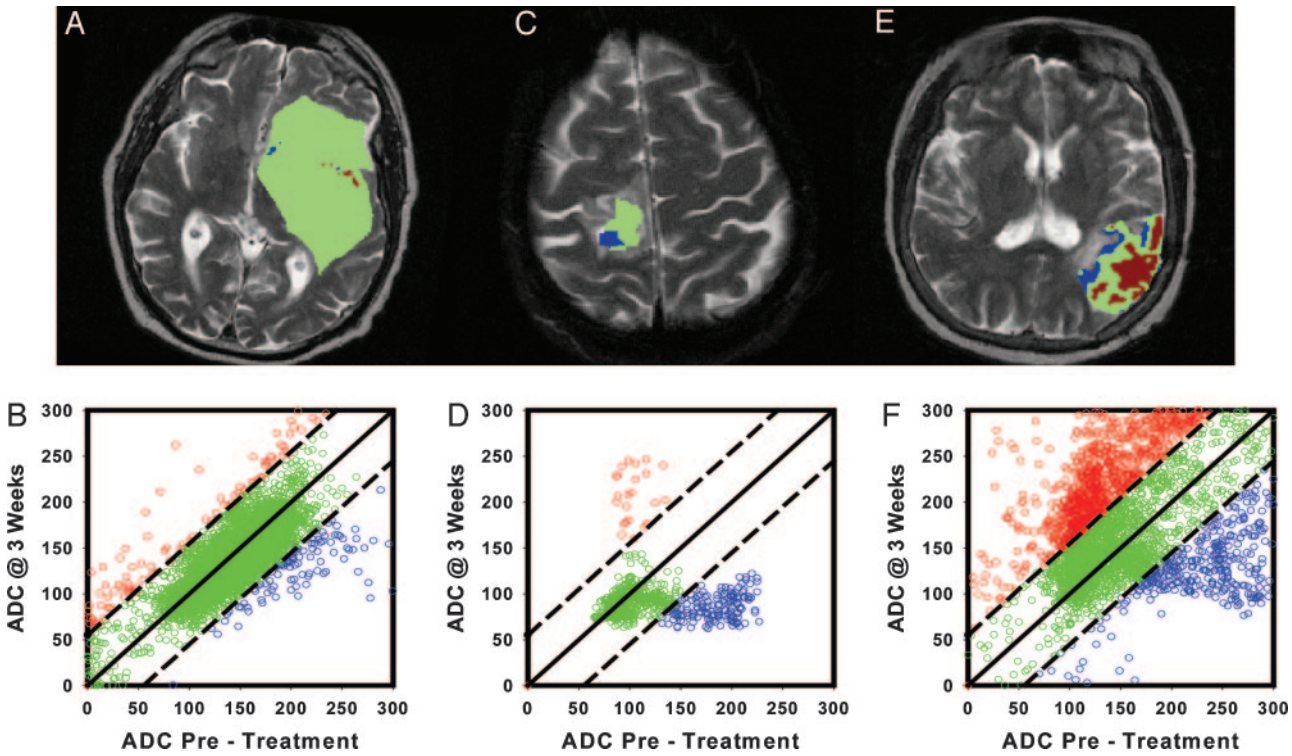

Fig. 2. MRI of three patients with oligodendrogliomas. MR image datasets obtained from three different patients diagnosed with anaplastic oligodendrogliomas. Images shown are at 3 weeks into a seven-week fractionated ionizing radiation regimen. Regions of interest were drawn for each tumor image by using anatomical images. (*A*, *C*, and *E*) Shown are the regional spatial distribution of ADC changes (fDMs) of a single slice through each tumor as color overlays for the PD, SD, and PR patients, respectively. The red pixels indicate areas of increased diffusion, whereas the blue and green pixels indicate regions of decreased and unchanged ADC, respectively. The scatter plots (*B*, *D*, and *F*) show quantitatively the distribution of ADC changes for the entire three-dimensional tumor volume for each corresponding patient (*A*, *C*, and *E*), respectively.

of ADC values from normal gray and white matter was correlated with the reference dataset by using linear least squares analysis. The 95% confidence intervals and standardized residuals were then determined from the results of the linear least squares analysis.

To test whether changes in diffusion images of brain tumors were correlated with patient radiographic outcome (PR, SD, and PD), the volumes V_R, V_B, and V_T ($V_T = V_R + V_B$) were then compared by using a one-way analysis of variance test (ANOVA). Wilson's scoring method (38) was then used to determine the sensitivity, specificity, and predictive values and accuracy of fDM for predicting outcomes.

Results

Patient Diagnosis, Therapy, and Outcome. A total of 20 patients with primary brain tumors were enrolled in the study as detailed in Table 1. Prescribed therapeutic interventions included chemotherapy, ionizing radiation, or combined therapy. Imaging was initiated just before the start of treatment and again during therapy at 3.2 ± 0.4 weeks (mean ± SD). Standard radiographic followup of tumor response beginning at 4 weeks after treatment classified 6 patients as PR, 6 patients as SD, and 8 patients as PD (Table 1).

Clinical Studies. Fig. 2 shows representative examples of fDMs overlayed on T2-weighted images from three patients with anaplastic oligodendrogliomas. Each of these patients received fractionated radiation therapy (total dose of 70 Gy in 2-Gy daily fractions 5 days a week over 7 weeks) and were subsequently classified as PD (Figs. 2 *A* and *B*), SD (Figs. 2 *C* and *D*), and PR (Figs. 2 *E* and *F*). The three colors used in these overlay images represent three different categories of diffusion values determined at 3 weeks after initiation of treatment. The red voxels indicate the regions of the tumor that had a significant increase in ADC (standardized residual > 1.96), the blue voxels indicate regions of significant reductions in ADC values (standardized residual < -1.96), and the green voxels represent tumor regions with no significant change ($-1.96 <$ standardized residual < 1.96). The total volume of the voxels within these three categories was then calculated for each patient at 3 weeks (PD patient, Fig. 2*B*; SD patient, Fig. 2*D*; and PR patient, Fig. 2*F*) and normalized against the total tumor volume to give three normalized tumor volume segments for each patient V_R, V_B, and V_G. Values for the PD patient ($V_R = 0.9\%$, $V_B = 1.1\%$ and $V_G = 98.0\%$), SD patient ($V_R = 2.7\%$, $V_B = 17.8\%$, and $V_G = 79.5\%$), and the PR patient ($V_R = 41.1\%$, $V_B = 15.2\%$, and $V_G = 43.7\%$) reveal significant differences between these patients that could be quantified at 3 weeks after initiation of therapy when less than half of the total radiation dose has been delivered and almost 2 months earlier than the radiographic response was defined in these patients.

Sensitivity and Specificity of fDMs. The box plots (Fig. 3) summarize the volumes of diffusion change obtained from fDM for each of the patient-response groups for the entire cohort of patients. The PR group had a $V_R = 33.2 \pm 5.9\%$ (mean ± SEM) (Fig. 3*A*) at 3 weeks posttreatment initiation (Fig. 3*A*), which was significantly larger ($P < 0.001$, power = 95.7%) than the SD ($V_R = 5.6 \pm 1.4\%$) and PD ($V_R = 1.1 \pm 0.4\%$) groups, which were also significantly different from each other ($P = 0.005$, power = 98.9%). As shown in Fig. 3*B*, the PR group had a $V_B = 4.0 \pm 2.8\%$ at 3 weeks posttreatment initiation, which was not significantly different from the V_B values of the SD and PD groups ($V_B = 10.6 \pm 3.2\%$, $P = 0.4$ and $V_B = 1.9 \pm 0.6\%$, $P = 0.2$, respectively). However, the V_B values were significantly different between the SD and PD patients ($P = 0.01$). The sum of the total

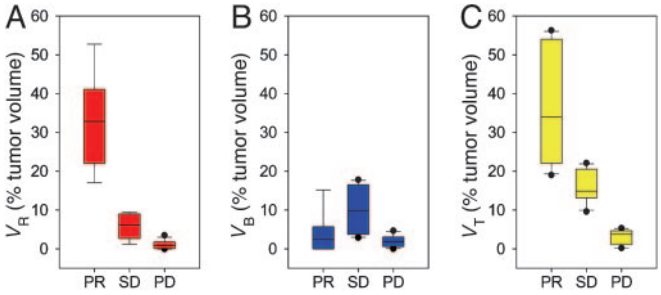

Fig. 3. Box plots summarizing fDM tumor volumes as a percent of total tumor volume for each patient group PR ($n = 6$), SD ($n = 6$), and PD ($n = 8$). (*A*) The volumes (percent of total) within the tumor that experienced significantly increased diffusion values (V_R). (*B*) The results for the tumor volume that had a significant decrease in diffusion values (V_B). (*C*) The total volume of tumor that had a significant change in ADC (V_T where $V_T = V_R + V_B$). Error bars reflect 95% confidence intervals.

diffusion changes ($V_T = V_R + V_B$) for the PR, SD, and PD were $36.6 \pm 6.8\%$, $16.2 \pm 2.1\%$, and $3.1 \pm 0.7\%$, respectively (Fig. 3*C*). The value of V_T for the PR group was significantly different from the PD ($P < 0.001$) and SD ($P = 0.02$) patient groups. In addition the V_T for the SD and PD groups were also significantly different from one another ($P < 0.001$, power = 99.9%).

Inspection of Fig. 3*A* reveals that the minimum value of V_R from the PR patient group was 16.5%. This value was outside the 95% confidence intervals and more than the maximum V_R values of 9.4% and 3.5% for the SD and PD patient groups, respectively. These readings show that increases in ADC values may be predictive of response (PR). The midpoint between the lower 95th percentile of PR patients and the upper 95th percentile of the SD patients was calculated to be 14% for V_R, which was used as the threshold for discrimination between groups. If the V_R derived from the ADC examination is >14% in a patient, it predicted the tumor response to be a PR. If V_R was <14%, it would be classified as either SD or PD. Fig. 3*C* reveals that total ADC changes (V_T) provides for the best discrimination between SD and PD patient populations. The midpoint between the 95% confidence intervals was calculated to be 8%, which was used as the threshold for discrimination between these groups (SD and PD).

On a patient-by-patient analysis, fDM had a 100% sensitivity [confidence interval (CI) 61–100] and a specificity of 100% (CI 78–100) for distinguishing PR patients from SD and PD patients by using a V_R threshold of 14%. In addition, a V_T threshold of 8% distinguished between SD and PD patients with 100% sensitivity (CI 61–100) and specificity (CI 68–100). The predictive values and overall accuracy for discriminating PR, SD, and PD patients at 3 weeks posttreatment initiation were found to be 100% for all 20 patients based on fDM analysis.

Discussion

There are currently no standard radiological methods for early assessment of tumor therapeutic efficacy during an interventional regimen, although several imaging approaches are under active evaluation (8–12). The early and accurate prediction of treatment response by using alterations in MRI tumor diffusion values may provide an opportunity to switch to a more beneficial therapy in patients who are nonresponders, thereby, minimizing the morbidity associated with prolonged and ineffective treatment. Moreover, early biomarkers, such as fDM, that reveal a therapeutic failure would also provide increased opportunities for these patients to be enrolled into clinical trials of experimental therapies with a higher Karnofsky performance status (39).

We found fDM analysis could be used to correctly identified PR, SD, and PD patients at 3 weeks into therapy. On a patient-by-patient basis, fDM had a sensitivity and a specificity of 100%. This current study significantly extends earlier work accomplished in rodent brain tumors (13, 20, 21, 23–25, 28) and the preliminary clinical observations in patients with brain and other cancer types (28–32). The advancement reported in this study was achieved by using coregistered MRI datasets along with thresholding allowing for quantification of change in treatment-induced tumor diffusion values. The predictive values and overall accuracy of fDM were found to be 100% for all 20 patients. This technique has the potential to provide significant clinical and cost benefits; however, larger prospective clinical trials will be needed to confirm these findings. Previously we had seen anecdotal changes by using mean ADC values in brain tumor patients (28); however, in this broader patient dataset, mean ADC values were not as predictive as the fDM approach reported here because of the lack of sensitivity of changes in ADC mean values in the presence of significant cellular heterogeneity within the tumor mass.

The SD patients had partial tumor volumes ($3\% \leq V_B \leq 21\%$) with significant decrease in diffusion in addition to volumes ($1\% \leq V_R \leq 9\%$) with increased diffusion at 3 weeks midtreatment (Fig. 3). These heterogeneous changes in tumor diffusion within the SD patient group exemplifies the dynamic and spontaneous spatial changes occurring in tumor morphology that can result from therapeutic intervention as depicted in Fig. 1 *A* and *B*. Thus, the sum of these overall changes (V_T) must be considered for predicting SD patients from PD brain tumor patients. Moreover, an ADC change averaged over the whole tumor is insensitive to spatial heterogeneity of treatment response. The fDM approach presented here provides a simple visual display of regions that appear to exhibit response and resistance to treatment, as well as offer the potential of a quantitative response grade by the scatter plot. Spatial maps of regional response/resistance have the added potential to adaptively guide spatially directed therapies (e.g., conformal radiation, brachytherapy, or direct injection of therapeutic agents) over the treatment course.

The diffusion imaging protocol used in this study is available on most modern clinical MR scanners. In major imaging centers, the collection of diffusion MR scans and the anatomical images for diagnosis and treatment of brain lesions is becoming more routine. The reduction, display, and analysis of fDM requires coregistration of pretreatment image datasets with a dataset collected during the initial course of treatment. Although coregistration and other specialized postprocessing software are not routinely available currently, these programs could easily be made available through an independent workstation, incorporated into existing picture archiving and communications systems, or added to the software associated with the clinical MR scanners. Investigations extending the application of fDM to solid tumors outside of the CNS (e.g., breast, liver, or head and neck tumors) are also feasible and would provide for an overall greater significant impact to the oncological imaging field and improved individualized care to a broader base of cancer patients.

In summary, the fDM analysis of longitudinal diffusion images reveals a potent depiction of the divergent response outcomes of tumors (PD, SD, and PR), thereby allowing for early detection of therapeutic-induced changes in tumor morphology. Significant changes in tumor ADC values occur after treatment initiation indicates that a patient is likely to show response to therapy (SD or PR). Moreover, a lack of change in tumor ADC values indicates a therapeutically unresponsive tumor (PD) and, thus, providing clinical information for which an alternative intervention can be prescribed. Finally, results from this patient population reveal that fDMs can serve as a valuable and powerful biomarker for the early assessment of tumor treatment response.

This work was supported in part by National Institutes of Health/National Cancer Institute Grants PO1CA85878, R24CA83099, and P50CA093990 and the Charles A. Dana Foundation.

1. Jemal, A., Tiwari, R. C., Murray, T., Ghafoor, A., Samuels, A., Ward, E., Feuer, E. J. & Thun, M. J. (2004) *CA Cancer J. Clin.* **54,** 8–29.
2. Laws, E. R., Parney, I. F., Huang, W., Anderson, F., Morris, A. M., Asher, A., Lillehei, K. O., Bernstein, M., Brem, H., Sloan, A., *et al.* (2003) *J. Neurosurg.* **99,** 467–473.
3. DeAngelis, L. M. (2001) *N. Engl. J. Med.* **344,** 114–123.
4. Walker, M. D., Alexander, E., Jr., Hunt, W. E., MacCarty, C. S., Mahaley, M. S., Jr., Mealey, J., Jr., Norrell, H. A., Owens, G., Ransohoff, J., Wilson, C. B., *et al.* (1978) *J. Neurosurg.* **49,** 333–343.
5. Chisholm, R. A., Stenning, S. & Hawkins, T. D. (1989) *Clin. Radiol.* **40,** 17–21.
6. James, K., Eisenhauer, E., Christian, M., Terenziani, M., Vena, D., Muldal, A. & Therasse, P. (1999) *J. Natl. Cancer Inst.* **91,** 523–528.
7. Macdonald, D. R., Cascino, T. L., Schold, S. C., Jr. & Cairncross, J. G. (1990) *J. Clin. Oncol.* **8,** 1277–1280.
8. Blankenberg, F., Mari, C. & Strauss, H. W. (2003) *Q. J. Nucl. Med.* **47,** 337–348.
9. Spence, A. M., Mankoff, D. A. & Muzi, M. (2003) *Neuroimaging Clin. N. Am.* **13,** 717–739.
10. Van de Wiele, C., Lahorte, C., Oyen, W., Boerman, O., Goethals, I., Slegers, G. & Dierckx, R. A. (2003) *Int. J. Radiat. Oncol. Biol. Phys.* **55,** 5–15.
11. Belhocine, T., Steinmetz, N., Green, A. & Rigo, P. (2003) *Ann. N.Y. Acad. Sci.* **1010,** 525–529.
12. Nelson, S. J. & Cha, S. (2003) *Cancer J.* **9,** 134–145.
13. Ross, B. D., Chenevert, T. L., Kim, B. & Ben-Joseph, O. (1994) *Q. Magn. Reson. Biol. Med.* **1,** 89–106.
14. Szafer, A., Zhong, J. & Gore, J. C. (1995) *Magn. Reson. Med.* **33,** 697–712.
15. Sykova, E., Svoboda, J., Polak, J. & Chvatal, A. (1994) *J. Cereb. Blood Flow Metab.* **14,** 301–311.
16. Norris, D. G., Niendorf, T. & Leibfritz, D. (1994) *NMR Biomed.* **7,** 304–310.
17. Sugahara, T., Korogi, Y., Kochi, M., Ikushima, I., Shigematu, Y., Hirai, T., Okuda, T., Liang, L., Ge, Y., Komohara, Y., *et al.* (1999) *J. Magn. Reson. Imaging* **9,** 53–60.
18. Lyng, H., Haraldseth, O. & Rofstad, E. K. (2000) *Magn. Reson. Med.* **43,** 828–836.
19. Guo, A. C., Cummings, T. J., Dash, R. C. & Provenzale, J. M. (2002) *Radiology* **224,** 177–183.
20. Ross, B. D., Ben-Joseph, O. & Chenevert, T. L. (1997) in *Magnetic Resonance Spectroscopy and Imaging in Neuorchemistry*, ed. Bachelard, H. (Plenum, New York), pp. 145–178.
21. Chenevert, T. L., McKeever, P. E. & Ross, B. D. (1997) *Clin. Cancer Res.* **3,** 1457–1466.
22. Chinnaiyan, A. M., Prasad, U., Shankar, S., Hamstra, D. A., Shanaiah, M., Chenevert, T. L., Ross, B. D. & Rehemtulla, A. (2000) *Proc. Natl. Acad. Sci. USA* **97,** 1754–1759.
23. Stegman, L. D., Rehemtulla, A., Hamstra, D. A., Rice, D. J., Jonas, S. J., Stout, K. L., Chenevert, T. L. & Ross, B. D. (2000) *Gene Ther.* **7,** 1005–1010.
24. Hakumaki, J. M., Poptani, H., Puumalainen, A. M., Loimas, S., Paljarvi, L. A., Yla-Herttuala, S. & Kauppinen, R. A. (1998) *Cancer Res.* **58,** 3791–3799.
25. Poptani, H., Puumalainen, A. M., Grohn, O. H., Loimas, S., Kainulainen, R., Yla-Herttuala, S. & Kauppinen, R. A. (1998) *Cancer Gene Ther.* **5,** 101–109.
26. Galons, J. P., Altbach, M. I., Paine-Murrieta, G. D., Taylor, C. W. & Gillies, R. J. (1999) *Neoplasia* **1,** 113–117.
27. Zhao, M., Pipe, J. G., Bonnett, J. & Evelhoch, J. L. (1996) *Br. J. Cancer* **73,** 61–64.
28. Chenevert, T. L., Stegman, L. D., Taylor, J. M., Robertson, P. L., Greenberg, H. S., Rehemtulla, A. & Ross, B. D. (2000) *J. Natl. Cancer Inst.* **92,** 2029–2036.
29. Mardor, Y., Pfeffer, R., Spiegelmann, R., Roth, Y., Maier, S. E., Nissim, O., Berger, R., Glicksman, A., Baram, J., Orenstein, A., *et al.* (2003) *J. Clin. Oncol.* **21,** 1094–1100.
30. Kremser, C., Judmaier, W., Hein, P., Griebel, J., Lukas, P. & de Vries, A. (2003) *Strahlenther. Onkol.* **179,** 641–649.
31. Hein, P. A., Kremser, C., Judmaier, W., Griebel, J., Pfeiffer, K. P., Kreczy, A., Hug, E. B., Lukas, P. & DeVries, A. F. (2003) *Eur. J. Radiol.* **45,** 214–222.
32. Ross, B. D., Moffat, B. A., Lawrence, T. S., Mukherji, S. K., Gebarski, S. S., Quint, D. J., Johnson, T. D., Junck, L., Robertson, P. L., Muraszko, K. M., *et al.* (2003) *Mol. Cancer Ther.* **2,** 581–587.
33. Turner, R., Le Bihan, D., Maier, J., Vavrek, R., Hedges, L. K. & Pekar, J. (1990) *Radiology* **177,** 407–414.
34. Basser, P. J., Mattiello, J. & LeBihan, D. (1994) *Biophys. J.* **66,** 259–267.
35. Moseley, M. E., Cohen, Y., Kucharczyk, J., Mintorovitch, J., Asgari, H. S., Wendland, M. F., Tsuruda, J. & Norman, D. (1990) *Radiology* **176,** 439–445.
36. Chenevert, T. L., Brunberg, J. A. & Pipe, J. G. (1990) *Radiology* **177,** 401–405.
37. Meyer, C. R., Boes, J. L., Kim, B., Bland, P. H., Zasadny, K. R., Kison, P. V., Koral, K., Frey, K. A. & Wahl, R. L. (1997) *Med. Image Anal.* **1,** 195–206.
38. Newcombe, R. G. (1998) *Stat. Med.* **17,** 857–872.
39. Lamborn, K. R., Chang, S. M. & Prados, M. D. (2004) *Neurooncology* **6,** 227–235.